

# GRASSMANNIAN DIFFUSION MAPS BASED DIMENSION REDUCTION AND CLASSIFICATION FOR HIGH-DIMENSIONAL DATA \*

KETSON R. M. DOS SANTOS<sup>†</sup>, DIMITRIS G. GIOVANIS<sup>†</sup>, AND MICHAEL D. SHIELDS<sup>†</sup>

**Abstract.** Diffusion Maps is a nonlinear dimensionality reduction technique used to embed high-dimensional data in a low-dimensional Euclidean space, where the notion of distance is due to the transition probability of a random walk over the dataset. However, the conventional approach is not capable to reveal the dataset underlying subspace structure, a useful information for machine learning applications such as object classification and face recognition. To circumvent this limitation, a novel nonlinear dimensionality reduction technique, referred to as Grassmannian Diffusion Maps, is developed herein relying on the affinity between subspaces represented by points on the Grassmann manifold. To this aim, a kernel matrix is used to construct the transition matrix of a random walk on a graph connecting points on the Grassmann manifold for posterior determination of the diffusion coordinates embedding the data in a low-dimensional Euclidean space. In this paper, three examples are considered to evaluate the performance of both conventional and Grassmannian Diffusion Maps. First, a “toy” example shows that the Grassmannian Diffusion Maps can identify a well-defined parametrization of points on the unit sphere, representing a Grassmann manifold. The second example shows that the Grassmannian Diffusion Maps outperforms the conventional Diffusion Maps in classifying elements, later recovered by a conventional clustering, of a dataset by their intrinsic characteristics. In the last example, a novel data classification/recognition technique is developed based on the construction of an overcomplete dictionary of reduced dimension whose atoms are given by the diffusion coordinates. A face recognition problem is solved considering face images subject to varying illumination conditions, changes in face expressions, and occurrence of occlusions. The technique presented high recognition rates (i.e., 95% in the best-case scenario) using a fraction of the data required by conventional methods.

**Key words.** Grassmann manifold, diffusion maps, dimension reduction, data classification, face recognition

**AMS subject classifications.** 53Z50, 14M15, 60J20

**1. Introduction.** Dimensionality reduction techniques play a fundamental role in the interpretation and characterization of high-dimensional data used in computationally intensive data-driven applications such as data compression [4, 11], data classification [43, 44], uncertainty quantification [12, 32, 13, 40], and biological sciences [36, 26, 25], just to mention few of them. Although linear dimensionality reduction methods (e.g., principal component analysis (PCA) [21]) suffice to extract features of the elements of a dataset, they fail to capture the intrinsic nonlinear geometric structure of the dataset itself. To circumvent this limitation, kernel-based techniques have been successfully employed in several applications taking advantage of the data similarity expressed on a connected graph designed over the dataset. Among these techniques one can include isometric mapping, also known as Isomap [34, 3], local linear embedding (LLE) [30, 9], T-distributed stochastic neighbor embedding (t-SNE) [37], kernel principal component analysis (Kernel PCA) [31]; Laplacian eigenmaps [6], and diffusion maps [7].

Many nonlinear dimensionality reduction techniques try to embed the data on a low-dimensional space where redundant and unimportant information can be neglected. It can be done by projecting the data on manifolds such as the Grassmann manifold [14, 45], a complete and connected smooth Riemannian manifold endowed

\*Preprint submitted to SIAM Journal of Scientific Computing.

<sup>†</sup>Department of Civil & Systems Engineering, Johns Hopkins University, Baltimore, MD, 21218, USA.

with a metric. Several applications using Grassmann manifold projections are found in the literature including the works by Turaga et al. [35], where statistical inference on the manifold is investigated to enhance the performance of activity recognition, video-based face recognition, and shape classification techniques. Moreover, Harandi et al. [18] used the Grassmann manifold theory to address problems in sparse coding and dictionary learning. Giovanis and Shields [12, 13] introduced a computationally efficient surrogate modeling scheme based on Grassmann manifold projections for prediction of high-dimensional stochastic models in a uncertainty quantification perspective.

Herein, a novel dimensionality reduction technique is introduced to reveal the global intrinsic structure of a dataset based on the underlying geometric structure of each data point. The technique has two steps, the first is a linear pointwise dimensionality reduction via Grassmannian projections, where the redundant and unimportant features of each element of a dataset are discarded. Next, a multipoint nonlinear dimensionality reduction via diffusion maps is considered aimed at learning the geometric structure of the Grassmann manifold on which the data lies. In this regard, a set of coordinates in the Euclidean space is obtained from the eigendecomposition of the transition matrix of a random walk on a graph connecting the points on the Grassmann manifold. In comparison with existing techniques, this novel approach does not need to perform a global dimensionality reduction to identify the basis spanning all the elements of a given dataset. Moreover, as the similarity between points in the dataset is defined by the affinity between their underlying subspaces and not by their topology in the ambient space, more robust data classifiers can be obtained.

This paper is organized as follows. In section 2, elements Grassmann manifold theory are introduced. The definitions of Stiefel and Grassmann manifolds are presented together with the definition of the tangent space and geodesic path, as well as definitions of the exponential and logarithmic maps. In section 3, the notion of distance is introduced based on the concept of principal angles between subspaces. Section 4 introduces the concept of a kernel on the Grassmann manifold, which is necessary for the development of the multipoint dimensionality reduction. In section 5, the Grassmannian diffusion maps (GDM) is introduced and the characteristics of the obtained diffusion coordinates are discussed. Section 6 introduces a novel data classification technique where the sparse representation-based classification method [42] is informed by the Grassmannian diffusion maps and data classification can be performed with a fraction of the amount of data used by some conventional techniques. In section 7, three examples are presented to corroborate the arguments presented in sections 5 and 6 and to assess the performance of the conventional and the Grassmannian diffusion maps.

**2. Grassmann manifold.** In this section, elements of differential geometry are exploited to describe the Stiefel and the Grassmann manifolds aiming at the development of a diffusion maps technique relying on Grassmannian kernels. First, let's consider the ambient space  $\mathbb{R}^n$ , where one can define a  $p$ -plane as the subspace of dimension  $p$  with  $0 < p < n$ , and a  $p$ -frame as an ordered set of  $p$  mutually orthonormal vectors in  $\mathbb{R}^n$  [2, 45]. The Stiefel manifold  $\mathcal{V}(p, n)$ , which is induced by the orthogonal group  $O(n)$  [2], is defined as follows.

**DEFINITION 2.1.** *The Stiefel manifold  $\mathcal{V}(p, n)$  is the set of  $p$ -frames in  $\mathbb{R}^n$  such that  $\mathcal{V}(p, n) = \{\mathbf{X} \in \mathbb{R}^{n \times p} : \mathbf{X}^T \mathbf{X} = \mathbf{I}_p\}$ .*

where  $\mathbf{I}_p \in \mathbb{R}^{p \times p}$  is the identity matrix and  $\mathbf{X} \in \mathbb{R}^{n \times p}$  is an orthonormal matrix. Moreover,  $\mathcal{V}(p, n)$  is a compact manifold with dimension given by  $\dim[\mathcal{V}(p, n)] = np - \frac{1}{2}p(p+1)$  [45]. Furthermore, the Stiefel manifold is a homogeneous space represented as a quotient space [45, 46], such that

$$(2.1) \quad \mathcal{V}(p, n) \cong \frac{O(n)}{O(n-p)}.$$

The right action of  $O(p)$  on  $\mathcal{V}(p, n)$  induces a homogeneous space with dimension  $p(n-p)$  known as the Grassmann manifold [45], whose definition is given next.

**DEFINITION 2.2.** *The Grassmann manifold (or Grassmannian)  $\mathcal{G}(p, n)$  is a set of  $p$ -planes in  $\mathbb{R}^n$  where a point on  $\mathcal{G}(p, n)$  is given by  $\mathcal{X} = \text{span}(\Psi)$  with  $\Psi \in \mathcal{V}(p, n)$ .*

Moreover,  $\mathcal{X}$  is identified as an equivalence class of  $n \times p$  matrices under orthogonal transformation of the Stiefel manifold [45, 46], such that.

$$(2.2) \quad \mathcal{G}(p, n) \cong \frac{O(n)}{O(n-p)O(p)} = \frac{\mathcal{V}(p, n)}{O(p)}.$$

For  $p = 1$  the Grassmann manifold  $\mathcal{G}(1, n)$  is a generalization of the projective space  $\mathbb{P}^{n-1}$  corresponding to the lines passing through the origin of the Euclidean space [19]. Further, a point  $\mathcal{X} = \text{span}(\Psi) \in \mathcal{G}(p, n)$  is invariant to the choice of basis such that  $\text{span}(\Psi) = \text{span}(\mathbf{R}\Psi)$ , where  $\mathbf{R} \in SO(p)$  with  $SO(p)$  being the special orthogonal group [45]. Herein, a point on the Grassmann manifold is an equivalence class defined by a point on the Stiefel manifold. Therefore, a representation of a point on the Grassmann manifold is given by an orthonormal matrix  $\Psi \in \mathbb{R}^{n \times p}$ .

**2.1. Grassmann manifold: Tangent space and geodesic path.** Due to the smoothness of  $\mathcal{G}(p, n)$  one can define tangent vectors at a given point  $\mathcal{X} \in \mathcal{G}(p, n)$  as an equivalence class of differentiable curves  $\gamma(t)$  passing through  $\mathcal{X}$ . In this regard, a tangent space  $\mathcal{T}_{\mathcal{X}}\mathcal{G}(p, n)$ , which is a flat inner-product space, is defined as follows [23, 39, 33].

**DEFINITION 2.3.** *The tangent space  $\mathcal{T}_{\mathcal{X}}\mathcal{G}(p, n)$  is the a set of all tangent vectors in  $\mathcal{X}$ , such that*

$$(2.3) \quad \mathcal{T}_{\mathcal{X}}\mathcal{G}(p, n) = \{\mathbf{\Gamma} \in \mathbb{R}^{n \times p} : \mathbf{\Gamma}^T \Psi = \mathbf{0}\}.$$

Moreover, the geodesic curve  $\gamma(t)$  on  $\mathcal{G}(p, n)$  has the following definition

**DEFINITION 2.4.** *The geodesic curve  $\gamma(t) : I \rightarrow \mathcal{G}(p, n)$ , is a differentiable curve on  $\mathcal{G}(p, n)$  that is locally length-minimizing with respect to a Riemannian metric.*

where  $I$  is an interval in  $\mathbb{R}$ . Further, the vectors tangent to  $\gamma(t)$  are covariantly constant, where  $\nabla_{\dot{\gamma}}\dot{\gamma}(t) = 0$  [47].

To develop a map from the manifold to the tangent space and vice-versa let's first restrict the interval  $I \in \mathbb{R}$  to  $I = [0, t]$  yielding a geodesic segment joining  $\gamma(0)$  to  $\gamma(t)$ . Therefore, using the Einstein summation convention and the Levi-Civita connection, one can make the covariant derivative of  $\dot{\gamma}$  equal to zero to obtain the geodesic equation [20, 33], such that

$$(2.4) \quad \ddot{\gamma}^\lambda + \Gamma_{\mu\nu}^\lambda \dot{\gamma}^\mu \dot{\gamma}^\nu = 0,$$

where  $\Gamma_{\mu\nu}^\lambda$  are the Christoffel symbols. Due to the local existence and uniqueness theorem for geodesics, one can say that given a point  $\mathcal{X}_0 \in \mathcal{G}(p, n)$  and a vector  $\dot{\mathcal{X}}_0 \in \mathcal{T}_{\mathcal{X}_0}\mathcal{G}(p, n)$  the geodesic exists and it is unique, such that  $\gamma(0) = \mathcal{X}_0$  and  $\dot{\gamma}(0) = \dot{\mathcal{X}}_0$ . This can be proven using the theory of ordinary differential equations [20, 29].

**2.2. Grassmann manifold: exponential and logarithmic maps.** Considering that the Grassmann manifold  $\mathcal{G}(p, n)$  is connected and complete as a metric space, one can define an exponential map  $\exp_{\mathcal{X}} : \mathcal{T}_{\mathcal{X}}\mathcal{G}(p, n) \rightarrow \mathcal{G}(p, n)$  from the tangent space to every point  $\mathcal{X} \in \mathcal{G}(p, n)$ . Consider two points  $\mathcal{X}_0 = \text{span}(\Psi_0)$  and  $\mathcal{X}_1 = \text{span}(\Psi_1)$  in  $\mathcal{G}(p, n)$ , and a tangent space  $\mathcal{T}_{\mathcal{X}_0}\mathcal{G}(p, n)$  with  $\Gamma \in \mathcal{T}_{\mathcal{X}_0}\mathcal{G}(p, n)$ . One can map  $\Gamma$  to  $\gamma(1) = \mathcal{X}_1$ , where  $\gamma(0) = \mathcal{X}_0$  and  $\dot{\gamma}(0) = \dot{\mathcal{X}}_0$  (see Fig. 1) [12, 33]. Letting  $\mathcal{X}_1$  be expressed by the orthonormal matrix  $\Psi_1$ , the exponential map can be written as:

$$(2.5) \quad \exp_{\mathcal{X}_0}(\Gamma) = \Psi_1.$$

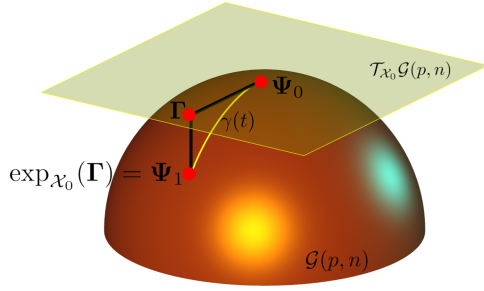


Figure 1: Exponential map of a point  $\Gamma \in \mathcal{T}_{\mathcal{X}}\mathcal{G}(1, 3)$  to the Grassmann manifold  $\mathcal{G}(1, 3)$ .

Expressing  $\Gamma$  by its thin singular value decomposition  $\Gamma = \mathbf{U}\mathbf{S}\mathbf{V}^T$  one can obtain the following expression after some algebraic manipulation [5].

$$(2.6) \quad \mathbf{U}\tan(\mathbf{S})\mathbf{V}^T = (\Psi_1 - \Psi_0\Psi_0^T\Psi_1)(\Psi_0^T\Psi_1)^{-1}.$$

If we define the matrix  $\mathbf{M} = (\Psi_1 - \Psi_0\Psi_0^T\Psi_1)(\Psi_0^T\Psi_1)^{-1}$  and express its thin SVD by  $\mathbf{M} = \mathbf{U}\mathbf{S}\mathbf{V}^T$ , the logarithmic map  $\log_{\mathcal{X}} : \mathcal{G}(p, n) \rightarrow \mathcal{T}_{\mathcal{X}}\mathcal{G}(p, n)$ , which is only invertible in the area close to  $\mathcal{X}_0$  [33], is given by

$$(2.7) \quad \log_{\mathcal{X}}(\Psi_1) = \mathbf{U}\tan^{-1}(\mathbf{S})\mathbf{V}^T.$$

The geodesic  $\gamma(t)$  parameterizes the curve connecting  $\Psi_0$  and  $\Psi_1$  on  $t \in [0, 1]$  with  $\gamma(0) = \Psi_0$  and  $\gamma(1) = \Psi_1$  such that their respective projections in the tangent space are connected by a straight line. It can thus be represented by the projection of this line in the tangent space by the exponential mapping, where  $\Gamma$  is expressed by its thin singular value decomposition  $\Gamma = \mathbf{U}\mathbf{S}\mathbf{V}^T$  [5]. Therefore, one can write  $\gamma(t)$  as

$$(2.8) \quad \gamma(t) = \text{span} [(\Psi_0\mathbf{V}\cos(t\mathbf{S}) + \mathbf{U}\sin(t\mathbf{S}))\mathbf{V}^T].$$

**3. Distances and metrics on the Grassmann manifold.** Points on the Grassmann manifold are intrinsically connected by smooth curves along which one can define a proper notion of distance. These distances are measured through the principal angles of the distance between the subspaces representing points on the Grassmann manifold, defined as follows.

DEFINITION 3.1. *Considering  $\mathbf{u}_i \in \text{span}(\Psi_u)$  and  $\mathbf{v}_i \in \text{span}(\Psi_v)$  on  $\mathcal{G}(k, n)$  and  $\mathcal{G}(l, n)$ , respectively, and letting  $p = \min(k, l)$ ; the principal angles  $0 \leq \theta_1 \leq \theta_2 \leq \dots \leq \theta_p \leq \pi/2$  are recursively obtained from  $\cos(\theta_i) = \max_{\mathbf{u}_i} \max_{\mathbf{v}_i} \mathbf{u}_i^T \mathbf{v}_i$  where  $\mathbf{u}_i$  and  $\mathbf{v}_i$  are orthonormal vectors.*

Alternatively, the cosine of the principal angles  $\theta_i \in [0, \pi/2]$  between the subspaces  $\text{span}(\Psi_u)$  and  $\text{span}(\Psi_v)$  can be computed from the singular values of  $\Psi_u^T \Psi_v$ . In this regard, one can write that

$$(3.1) \quad \Psi_u^T \Psi_v = \bar{\mathbf{U}} \bar{\mathbf{S}} \bar{\mathbf{V}}^T,$$

where  $\bar{\mathbf{U}} \in O(k)$ ,  $\bar{\mathbf{V}} \in O(l)$ , and  $\bar{\mathbf{S}} = \text{diag}(\sigma_1, \sigma_2, \dots, \sigma_p)$ , with  $p = \min(k, l)$ . Thus, the principal angles are computed as  $\theta_i = \cos^{-1}(\sigma_i)$  [24].

In fact, it has been shown that any measure of distance on the Grassmann manifold must be a function of the principal angles as stated in the following theorem (repeated from [41, 46]).

THEOREM 3.2. *Any notion of distance between  $k$ -dimensional subspaces in  $\mathbb{R}^n$  that depends only on the relative positions of the subspaces, i.e., invariant under any rotation in  $O(n)$ , must be a function of their principal angles. To be more specific, if a distance  $d : \mathcal{G}(k, n) \times \mathcal{G}(k, n) \rightarrow [0, \infty)$  satisfies  $d(Q \cdot \Psi_0, Q \cdot \Psi_1) = d(\Psi_0, \Psi_1)$  for all  $d(\Psi_0, \Psi_1) \in \mathcal{G}(k, n)$  and all  $Q \in O(n)$ , where  $Q \cdot \Psi_0 := \text{span}(Q\Psi_0) \in \mathcal{G}(k, n)$ , then  $d$  must be a function of  $\theta_i(\Psi_0, \Psi_1), i = 1, \dots, k$ .*

Perhaps the most common distance, the geodesic distance  $d_{\mathcal{G}(p,n)}(\Psi_0, \Psi_1)$  between two points  $\mathcal{X}_0 = \text{span}(\Psi_0)$  and  $\mathcal{X}_1 = \text{span}(\Psi_1)$  on  $\mathcal{G}(p, n)$ , corresponds to the distance over the geodesic  $\gamma(t)$  parameterized by  $t \in [0, 1]$  and it is given by [41, 45, 12]

$$(3.2) \quad d_{\mathcal{G}(p,n)}(\Psi_0, \Psi_1) = \|\Theta\|_2,$$

where  $\Theta = (\theta_1, \theta_2, \dots, \theta_p)$  is the vector of principal angles. This notion of distance, using the arc-length metric, between two subspaces in  $\mathcal{G}(2, 3)$  is represented in the unit semi-sphere in Fig. 2. Several definitions of distance/metrics on  $\mathcal{G}(p, n)$  can be found in the literature (see [45] for detailed information) and are listed in Table 1.

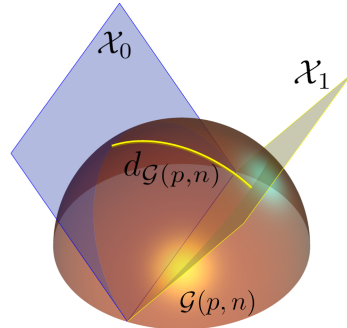


Figure 2: Geodesic distance between subspaces  $\mathcal{X}_0$  and  $\mathcal{X}_1$  of  $\mathbb{R}^2$  on  $\mathcal{G}(2, 3)$ .

Table 1: Distances/metrics on the Grassmann manifold

	<i>Principal angles</i>	<i>Orthonormal basis</i>
Asimov	$\theta_p$	$\cos^{-1} \ \Psi_0^T \Psi_1\ _2$
Binet-Cauchy	$(1 - \prod_{i=1}^p \cos^2 \theta_i)^{1/2}$	$\left[1 - (\det \Psi_0^T \Psi_1)^2\right]^{1/2}$
Arc-length	$(\sum_{i=1}^p \theta_i^2)^{1/2}$	$\ \cos^{-1} \Sigma\ _F$
Chordal	$(\sum_{i=1}^p \sin^2 \theta_i)^{1/2}$	$\frac{1}{\sqrt{2}} \ \Psi_0 \Psi_0^T - \Psi_1 \Psi_1^T\ _F$
Procrustes	$(2 \sum_{i=1}^p \sin^2 \frac{\theta_i}{2})^{1/2}$	$\ \Psi_0 \mathbf{U} - \Psi_1 \mathbf{V}\ _F$
Projection	$\sin \theta_p$	$\ \Psi_0 \Psi_0^T - \Psi_1 \Psi_1^T\ _2$
Spectral	$2 \sin \frac{\theta_p}{2}$	$\ \Psi_0 \mathbf{U} - \Psi_1 \mathbf{V}\ _2$

When defining a distance, it is often important that the distance be provided in terms of a metric, which formalizes the notation of distance on the manifold, and is defined next.

**DEFINITION 3.3.** *A metric on the Grassmann manifold is a function  $d : \mathcal{G}(k, n) \times \mathcal{G}(k, n) \rightarrow [0, \infty)$  where  $[0, \infty)$  is the set of non-negative real numbers and for all  $\mathcal{X}_0 = \text{span}(\Psi_0)$ ,  $\mathcal{X}_1 = \text{span}(\Psi_1)$ ,  $\mathcal{X}_2 = \text{span}(\Psi_2) \in \mathcal{G}(k, n)$ , the following three conditions are satisfied:*

1.  $d(\mathcal{X}_0, \mathcal{X}_1) = 0 \Leftrightarrow \mathcal{X}_0 = \mathcal{X}_1$  (*identity of indiscernibles*)
2.  $d(\mathcal{X}_0, \mathcal{X}_1) = d(\mathcal{X}_1, \mathcal{X}_0)$  (*symmetry*)
3.  $d(\mathcal{X}_0, \mathcal{X}_1) \leq d(\mathcal{X}_0, \mathcal{X}_2) + d(\mathcal{X}_2, \mathcal{X}_1)$  (*triangle inequality*)

The formalism of a metric on the manifold can be useful in properly defining a distance. This can be seen, for example, by observing that the value  $\sin \theta_1$  is sometimes called the max correlation distance or spectral distance [46], but it is not a distance in the sense of a metric because it can be zero for a pair of distinct subspaces. Clearly this is undesirable.

**4. Grassmannian kernels.** Although the notions of distance and similarity are connected, they are not interchangeable. The similarity is encoded by positive semi-definite kernels on a graph and it is maximized when the distance, which is a measure of dissimilarity, is equal to zero. As a kernel defines a similarity measure with an inner product representation, the embedding of Grassmannians into Hilbert spaces, where a Euclidean structure is identified, can be performed using Grassmannian kernels. In this regard, one can resort to the following definition of real-valued positive semi-definite kernels.

**DEFINITION 4.1.** *A real symmetric map is a real-valued positive semi-definite kernel if  $\sum_{i,j} c_i c_j k(x_i, x_j) \leq 0$ , with  $x \in \mathcal{X}$  and  $c_i \in \mathbb{R}$ .*

Therefore, a Grassmannian kernel can be defined as

**DEFINITION 4.2.** *A map  $k : \mathcal{G}(p, n) \times \mathcal{G}(p, n) \rightarrow \mathbb{R}$  is a Grassmannian kernel if it is invariant to the choice of basis and positive semi-definite.*

In kernel-based dimensionality reduction techniques, there are many commonly used kernels defined on Euclidean spaces. The Gaussian kernel is perhaps the most popular and is given by,

$$(4.1) \quad k(\mathbf{X}_i, \mathbf{X}_j) = \exp\left(-\frac{\|\mathbf{X}_i - \mathbf{X}_j\|_2^2}{4\varepsilon}\right),$$

where  $\mathbf{X}_i$  and  $\mathbf{X}_j$  are data points in the ambient Euclidean space and  $\varepsilon$  is the parameter controlling the spread of the kernel tails. It could be tempting to simply substitute the Euclidean norm in the definition of the Gaussian kernel by a metric on the Grassmann manifold. However, this procedure yields a non positive semi-definite, although symmetric, kernel [19]. Several families of Grassmannian kernels, with different characteristics, are proposed in the literature (see [16, 17, 19]); however, the most popular positive semi-definite kernels are the Binet-Cauchy and Projection kernels. These kernels can be employed on the transformation of problems defined on the Grassmann manifold to problems on Hilbert spaces. Next, a detailed analysis of both kernels is presented.

**4.1. Embedding the Grassmann manifold.** The embedding of the Grassmann manifold into Hilbert spaces is analyzed herein. In particular, the Plücker and the projection embeddings are considered to show how to construct the the Binet-Cauchy and projection kernels, respectively.

**4.1.1. Binet-Cauchy kernel: Plücker embedding.** The Plücker embedding plays an important role in embedding the Grassmann manifold  $\mathcal{G}(p, n)$  into the projective space  $\mathbb{P}(\wedge^p \mathbb{R}^n)$ , where the exterior product  $\wedge^p \mathbf{V}$  is the  $k$ -th product of a vector space  $\mathbf{V}$ . Thus, the Plücker embedding  $P : \mathcal{G}(p, n) \rightarrow \mathbb{P}(\wedge^p \mathbb{R}^n)$  can be defined as  $P(\Psi) = [\psi_1 \wedge \psi_2 \wedge \dots \wedge \psi_p]$ . One can easily show that the Plücker coordinates of  $\Psi \in \mathcal{G}(p, n)$  are the  $p \times p$  minors, matrices obtained by taking  $p$  rows out of  $n$  of  $\mathbf{X}$ . This property can be used to define an inner product over  $\mathbb{P}(\wedge^p \mathbb{R}^n)$  by taking advantage of compound matrices, such that the elements of the  $q$ -th compound matrix  $C_q(\Psi)$  of a matrix  $\Psi$  are the minors of  $\Psi$  of order  $q$  arranged in a lexicographic order [19]. Thus, using the Binet-Cauchy theorem [38, 19] and given the points  $\mathcal{X}_0 = \text{span}(\Psi_0) \in \mathcal{G}(n, k)$  and  $\mathcal{X}_1 = \text{span}(\Psi_1) \in \mathcal{G}(n, l)$ , one can write  $C_q(\Psi_0^T \Psi_1) = C_q(\Psi_0)^T C_q(\Psi_1)$ . Therefore,  $k_{bc}(\Psi_0, \Psi_1) = \text{Tr}[C_q(\Psi_0)^T C_q(\Psi_1)] = \text{Tr}[C_q(\Psi_0^T \Psi_1)] = \det(\Psi_0^T \Psi_1)$ , which can be defined as an inner product for the Plücker embedding. One of the problems with this definition of inner product is that the sign of  $\det(\cdot)$  can change when columns of  $\Psi_0$  are permuted. This limitation can be circumvented by taking the square value of  $\det(\Psi_0^T \Psi_1)$ . Thus, one can write  $k_{bc}(\Psi_0, \Psi_1) = \det(\Psi_0^T \Psi_1)^2$ . In reality several families of kernels are constructed based on the Binet-Cauchy theorem. It includes the polynomial generalizations  $k_{bc}(\Psi_0, \Psi_1) = [\beta + \det(\Psi_0^T \Psi_1)]^\alpha$  (see [19] for a detailed description). Herein, the adopted definition of the Binet-Cauchy kernel is given by

$$(4.2) \quad k_{bc}(\Psi_0, \Psi_1) = \det(\Psi_0^T \Psi_1)^2,$$

whose relation with the principal angles is given by [16, 19]

$$(4.3) \quad k_{bc}(\Psi_0, \Psi_1) = \prod_{i=1}^p \cos^2(\theta_i).$$

**4.1.2. Projection kernel: projection embedding.** The projection kernel is defined straightforwardly using the projection embedding  $\Pi : \mathcal{G}(p, n) \rightarrow \mathbb{R}^{n \times n}$  given by  $\Pi(\Psi) = \Psi \Psi^T$ . This map corresponds to a diffeomorphism, a differentiable mapping with a continuous differentiable inverse, from the Grassmann manifold to the set of rank  $p$  symmetric orthogonal projection matrices. Therefore, a natural definition of inner product for the projection embedding is given by  $\langle \Psi_0, \Psi_1 \rangle_\Pi = \text{Tr}[\Pi(\Psi_0)^T \Pi(\Psi_1)] = \|\Psi_0^T \Psi_1\|_F^2$ . As for the Binet-Cauchy kernel, several families

can be obtained using the projection embedding, however, herein the projection kernel is defined as

$$(4.4) \quad k_{pr}(\Psi_0, \Psi_1) = \|\Psi_0^T \Psi_1\|_F^2,$$

whose relation with the principal angles is given by [16, 19]

$$(4.5) \quad k_{pr}(\Psi_0, \Psi_1) = \sum_{i=1}^p \cos^2(\theta_i).$$

**4.2. Grassmannian kernel dimensionality.** The properties of the projection and Binet-Cauchy kernels that may have some influence on their selection for a specific application are investigated in this section. The relationship between the dimensionality of the Grassmann manifold  $\mathcal{G}(p, n)$ , and the entries of the kernel matrix, is analyzed based on the distribution of the principal angles between random matrices. In this regard, let's first assume  $p = 1$  in Eqs. (4.2 - 4.5). One can easily show that  $k_{pr}(\Psi_i, \Psi_j) = k_{bc}(\Psi_i, \Psi_j)$  for two different subspaces  $\mathcal{X}_i = \text{span}(\Psi_i)$  and  $\mathcal{X}_j = \text{span}(\Psi_j)$ . However, more attention should be paid to the influence of  $p$  and  $n$ , when  $1 < p < n$  and  $n > 1$ , in the similarity between distinct points in the same manifold. Next, a more detailed analysis is presented for both the projection and Binet-Cauchy kernels. Further, the lemmas presented in this section are developed considering two subspaces  $\mathcal{X}_i = \text{span}(\Psi_i)$  and  $\mathcal{X}_j = \text{span}(\Psi_j)$  chosen from the uniform distribution on  $\mathcal{G}(p, n)$ , which is an invariant distribution on the Grassmann manifold. Moreover, the entries of the kernel matrix are denoted by  $k_{ij} = k(\Psi_i, \Psi_j)$ , where for an ensemble of random subspaces the expected value is denoted by  $\bar{k}_{ij}$ .

**4.2.1. Kernel dimensionality: projection kernel.** The following lemmas are used to show that the expected values of the entries of the kernel matrix  $k_{pr}(\Psi_i, \Psi_j)$  have a well-defined functional relationship with both  $p$  and  $n$ .

LEMMA 4.3. *Given two random subspaces  $\mathcal{X}_i = \text{span}(\Psi_i)$  and  $\mathcal{X}_j = \text{span}(\Psi_j)$  on  $\mathcal{G}(p, n)$ , if  $i = j$  the entries in the diagonal of  $k_{pr}(\Psi_i, \Psi_j)$  are given by  $k_{ii} = p$ .*

*Proof.* The proof of lemma 4.3 is trivial because  $\cos^2(\theta_i) = 1$  for  $i = 1, \dots, p$  in Eq. (4.5).  $\square$

On the other hand, if  $i \neq j$ , the following lemma holds.

LEMMA 4.4. *Given two random subspaces  $\mathcal{X}_i = \text{span}(\Psi_i)$  and  $\mathcal{X}_j = \text{span}(\Psi_j)$  on  $\mathcal{G}(p, n)$ , if  $1 \leq p \leq n$  the expected value  $\bar{k}_{ij}(p, n)$  of the off-diagonal entries of  $k_{pr}(\Psi_i, \Psi_j)$  has the following functional form*

$$(4.6) \quad \bar{k}_{ij}(p, n) = \frac{p^2}{n}.$$

*Proof.* A fixed subspace  $\mathcal{X}_i = \text{span}(\Psi_i)$  and a subspace  $\mathcal{X}_j = \text{span}(\Psi_j)$  chosen from the uniform distribution on  $\mathcal{G}(p, n)$ , which is an invariant distribution on the Grassmann manifold, are given by

$$(4.7) \quad \Psi_i = \begin{bmatrix} \mathbf{I}_p \\ \mathbf{0}_{n-p,p} \end{bmatrix},$$

and

$$(4.8) \quad \hat{\Psi}_j = \begin{bmatrix} \mathbf{A} \\ \mathbf{B} \end{bmatrix},$$

where  $\mathbf{I}_p$  is a  $p \times p$  identity matrix,  $\mathbf{0}_{n-p,p}$  is a  $(n-p) \times p$  null matrix,  $\mathbf{A} \in \mathbb{R}^{p \times p}$  and  $\mathbf{B} \in \mathbb{R}^{(n-p) \times p}$  are i.i.d. Gaussian matrices, since the Gaussian distribution is invariant under orthogonal group transformation [1]. Further, the orthonormalization of  $\hat{\Psi}_j$  is given by  $\Psi_j = \hat{\Psi}_j (\mathbf{A}^T \mathbf{A} + \mathbf{B}^T \mathbf{B})$ . Thus,  $\sigma_i^2 = \cos^2(\theta_i)$ , with  $i = 1, \dots, p$ , are equal to the eigenvalues values  $\{\lambda_i\}_{i=1}^p$  of  $(\mathbf{A}^T \mathbf{A} + \mathbf{B}^T \mathbf{B})^{-1/2} \mathbf{A}^T \mathbf{A} (\mathbf{A}^T \mathbf{A} + \mathbf{B}^T \mathbf{B})^{-1/2}$ . Or equivalently given by the eigenvalues of  $\mathbf{W} = (\mathbf{L}^{-1})^T \mathbf{A}^T \mathbf{A} \mathbf{L}^{-1}$ , where  $\mathbf{A}^T \mathbf{A} + \mathbf{B}^T \mathbf{B} = \mathbf{L}^T \mathbf{L}$  is the Cholesky decomposition of  $\mathbf{A}^T \mathbf{A} + \mathbf{B}^T \mathbf{B}$ . As  $\mathbf{L}$  has a beta distribution  $\text{Beta}_p[p/2, (n-p)/2]$ , the joint probability density function (PDF) of  $\{\lambda_i\}_{i=1}^p$ , when  $n \geq 2p$ , is given by [27, 10, 1]

$$(4.9) \quad f(\lambda_1, \dots, \lambda_p) = \frac{\pi^{p^2/2} \Gamma_p(n/2)}{\Gamma_p^2(p/2) \Gamma_p((n-p)/2)} \prod_{i < j} |\lambda_i - \lambda_j| \prod_{i=1}^p \lambda_i^{-1/2} (1 - \lambda_i)^{\frac{1}{2}(n-2p-1)},$$

where  $\Gamma_m(\cdot)$  is the multivariate gamma function [27, 1]. Therefore, the PDF of the largest principal angle between the subspaces  $\mathcal{X}_i$  and  $\mathcal{X}_j$  randomly chosen from  $\mathcal{G}(p, n)$  can be obtained (see [1] for a detailed presentation). At this point, our interest is focused on the case  $p = 1$ , whose PDF of the cosine square of the unique principal angle is given by

$$(4.10) \quad f(\lambda) = \frac{\Gamma\left(\frac{n}{2}\right)}{\Gamma\left(\frac{1}{2}\right) \Gamma\left(\frac{n-1}{2}\right)} \lambda^{-\frac{1}{2}} [1 - \lambda]^{\frac{n-3}{2}},$$

where  $\Gamma(\cdot)$  is the gamma function,  $\lambda = \cos^2(\theta_1)$ . The mean and variance are given by

$$(4.11) \quad \mathbb{E}[\lambda] = \frac{1}{n},$$

and

$$(4.12) \quad \text{Var}[\lambda] = \frac{2(n-1)}{n^2(n+2)}.$$

Assuming that  $\Psi_i^T \Psi_j = \mathbf{U} \mathbf{S} \mathbf{V}^T$ , where  $\mathbf{S} = \text{diag}([\sigma_1, \dots, \sigma_p])$  and considering that  $\Psi_i$  and  $\Psi_j$  are orthonormal matrices, one can use the following identity

$$(4.13) \quad \sum_{i=1}^p \sigma_i^2 = \text{Tr}(\Psi_i \Psi_i^T \Psi_j \Psi_j^T).$$

Therefore, considering that  $\mathbf{Z} = \Psi_i \Psi_i^T \Psi_j \Psi_j^T$  one can write Eq. (4.13) for every realization  $\xi$  of  $\Psi_j$ , such that

$$(4.14) \quad \sum_{i=1}^p \sigma_i^2(\xi) = \sum_{i=1}^p \mathbf{Z}_{ii}(\xi).$$

Taking the expectation of both sides of Eq. (4.14) one can obtain

$$(4.15) \quad \sum_{i=1}^p \mathbb{E}[\sigma_i^2(\xi)] = \sum_{k=1}^p \mathbb{E}[\mathbf{Z}_{kk}(\xi)].$$

From the definition of  $\mathbf{Z}$  one can obtain

$$(4.16) \quad \mathbf{Z}_{kk}(\xi) = \sum_{l=1}^p \Psi_{j,(k,l)}^2,$$

where  $\Psi_{j,(k,l)}$  corresponds to the element  $(k,l)$  of  $\Psi_j$ . Therefore, as the columns of  $\Psi_j$  are orthonormal vectors in  $\mathbb{R}^n$ , the components of the vector  $\Psi_{j,(:,l)}$  are equal to the cosine of the direction angles  $\alpha_k$  between  $\Psi_j$  and the component in the coordinate axis  $k$  with  $k = 1, \dots, n$ . It is clear that the dot product of unit vectors uniformly distributed on the sphere  $\mathbb{S}^n$  has a beta distribution; thus, assuming that  $\Psi_{j,(k,l)}$  are i.i.d. one can find that  $(\Psi_{j,(k,l)} + 1)/2 \sim \text{Beta}[(n-1)/2, (n-1)/2]$  [15]. As  $E[\Psi_{j,(k,l)}] = 0$ , the variance of  $\Psi_{j,(k,l)}$  is given by

$$(4.17) \quad \text{Var}[\Psi_{j,(k,l)}] = E[\Psi_{j,(k,l)}^2] = \frac{1}{n}.$$

Moreover, if the columns of  $\Psi_j$  are orthonormal vectors in  $\mathbb{R}^n$ , the components of the vector  $\Psi_{j,(:,l)}$  are equal to the cosine of the direction angles  $\alpha_k$  between  $\Psi_j$  and the component in the coordinate axis  $k$  with  $k = 1, \dots, n$ . Therefore,  $\Psi_{j,(k,l)}^2 = \cos^2(\alpha_k)$ . Thus, one can observe that the results presented in Eqs. (4.10 - 4.12) are valid for  $\lambda = \cos^2(\alpha_k)$ . Therefore, from Eq. (4.16) one can show that

$$(4.18) \quad E[\mathbf{Z}_{kk}(\xi)] = \frac{p}{n}.$$

Substituting Eq. (4.18) in Eq. (4.15) one can easily show that

$$(4.19) \quad \bar{k}_{ij}(p, n) = \sum_{i=1}^p E[\sigma_i^2(\xi)] = \frac{p^2}{n}. \quad \square$$

A Monte Carlo simulation is performed to verify the consistency of the result presented in this section. In this regard, 3,000 random matrices  $\hat{\Psi}_j$  are sampled from a Gaussian distribution, as presented in the proof of lemma 4.4, for each value of  $p = 1, \dots, 19$ , with  $n = 20$ . Thus, it is shown in Fig. 3a that the result of lemma 4.4 holds.

**4.2.2. Kernel dimensionality: Binet-Cauchy kernel.** From Eq. (4.2) the Binet-Cauchy kernel corresponds to the product of the square of the singular values of  $\Psi_i^T \Psi_j$ . In this regard, the values of the off-diagonal elements of  $k_{bc}(\Psi_i, \Psi_j)$  are governed by those singular values larger than zero and lower than one. Therefore, one can start this analysis assuming that the following lemma holds.

**LEMMA 4.5.** *Given two random subspaces  $\mathcal{X}_i$  and  $\mathcal{X}_j$  on  $\mathcal{G}(p, n)$ , if  $p \geq n/2$  the multiplicity of the principal angle  $\theta = 0$  between them is equal to  $2p - n$ .*

*Proof.* Assuming that  $\mathcal{X}_i = \text{span}(\Psi_i)$  and  $\mathcal{X}_j = \text{span}(\Psi_j)$  and considering that the multiplicity of the principal angle  $\theta = 0$  between  $\mathcal{X}_i$  and  $\mathcal{X}_j$  is equal to  $\dim(\mathcal{X}_i \cap \mathcal{X}_j)$  one can use the following expression

$$(4.20) \quad \dim(\mathcal{X}_i \cap \mathcal{X}_j) = \dim(\mathcal{X}_i) + \dim(\mathcal{X}_j) - \dim(\mathcal{X}_i + \mathcal{X}_j),$$

or alternatively,

$$(4.21) \quad \dim(\mathcal{X}_i \cap \mathcal{X}_j) = \text{rank}(\Psi_i) + \text{rank}(\Psi_j) - \text{rank}([\Psi_i, \Psi_j]). \quad \square$$

As  $\mathcal{X}_i, \mathcal{X}_j \in \mathcal{G}(p, n)$ ,  $\text{rank}(\Psi_i) = \text{rank}(\Psi_j) = p$ . Moreover,  $\text{rank}([\Psi_i, \Psi_j]) = n$ , since  $p \geq n/2$ . Therefore,  $\dim(\mathcal{X}_i \cap \mathcal{X}_j) = 2p - n$ .

The result presented in lemma 4.5 is useful to show that  $p = n/2$  corresponds to the largest value of  $p$  where all the singular values of  $\Psi_i^T \Psi_j$  are strictly less than 1. Therefore, the number of positive singular values smaller than one is equal to  $p$  if  $1 \leq p < n/2$ ; and  $n-p$  if  $n/2 \leq p < n$ . Thus, one can conclude that when  $p = n/2$  the expected value of the off-diagonal entries  $\bar{k}_{ij}(p, n)$  of  $k_{bc}(\Psi_i, \Psi_j)$  is minimal. Next, a lemma for the diagonal elements of the Binet-Cauchy kernel matrix  $k_{bc}$  is presented.

LEMMA 4.6. *Given two random subspaces  $\mathcal{X}_i = \text{span}(\Psi_i)$  and  $\mathcal{X}_j = \text{span}(\Psi_j)$  on  $\mathcal{G}(p, n)$ , if  $i = j$  the entries in the diagonal of  $k_{bc}(\Psi_i, \Psi_j)$  are given by  $k_{ii} = 1$ .*

*Proof.* The proof of lemma 4.6 is trivial because  $\cos^2(\theta_i) = 1$  for  $i = 1, \dots, p$  in Eq. (4.3).  $\square$

One can start the analysis of the off-diagonal entries of the Binet-Cauchy kernel matrix from the trivial cases. Considering two random subspaces  $\mathcal{X}_i$  and  $\mathcal{X}_j$  one can easily show that for  $p = 1$  the expected value of the off-diagonal entries of the Binet-Cauchy kernel is given by  $\bar{k}_{ij}(p, n) = 1/n$ , as in the projection kernel. On the other hand, for  $p = n$ , which is an extreme case used for theoretical purposes only, one can observe that  $k_{ij}(p) = 1$  because all the principal angles are equal to zero. Therefore, in the extreme cases both kernels have similar behavior. More generally, one can show that the expected values of the off-diagonal entries of the Binet-Cauchy kernel can be obtained using the joint probability density function in Eq. (4.9). However, this calculation is cumbersome and an upper bound for the expected value of the off-diagonal entries of the Binet-Cauchy kernel matrix can be defined as presented in the following lemma.

LEMMA 4.7. *Given two random subspaces  $\mathcal{X}_i = \text{span}(\Psi_i)$  and  $\mathcal{X}_j = \text{span}(\Psi_j)$  on  $\mathcal{G}(p, n)$  the expected value  $\bar{k}_{ij}(p, n)$  of the off-diagonal entries of  $k_{bc}(\Psi_i, \Psi_j)$  has the following upper bound*

$$(4.22) \quad \bar{k}_{ij}(p, n) \leq \begin{cases} \left(\frac{p}{n}\right)^p, & \text{if } 1 \leq p < \frac{n}{2} \\ \left(\frac{n-p}{n}\right)^{n-p}, & \text{if } \frac{n}{2} \leq p < n \end{cases}.$$

*Proof.* Considering the matrices  $\Psi_i$  and  $\Psi_j$ , presented in the proof of lemma 4.4, as bases of both subspaces  $\mathcal{X}_i$  and  $\mathcal{X}_j$ , respectively; and using the inequality of arithmetic and geometric means (AM-GM inequality) [8] one can observe that

$$(4.23) \quad \left(\prod_{i=1}^p \mathbb{E}[\sigma_i^2(\xi)]\right)^{\frac{1}{p}} \leq \frac{1}{p} \sum_{i=1}^p \mathbb{E}[\sigma_i^2(\xi)].$$

From lemma 4.4 one can say that  $\mathbb{E}[\sigma_i^2(\xi)]$  with  $i = 1, \dots, p$  is equal to  $p/n$ . Thus, one can write

$$(4.24) \quad \left(\prod_{i=1}^p \mathbb{E}[\sigma_i^2(\xi)]\right)^{\frac{1}{p}} \leq \frac{p}{n}.$$

Therefore, the expected value of the off-diagonal entries of the Binet-Cauchy kernel has an upper bound given by

$$(4.25) \quad \bar{k}_{ij}(p, n) \leq \left(\frac{p}{n}\right)^p,$$

if  $p < n/2$ . On the other hand, if  $n/2 \leq p < n$  the upper bound is given by

$$(4.26) \quad \bar{k}_{ij}(p) \leq \left(\frac{n-p}{n}\right)^{n-p}.$$

In fact, Eq. (4.26) holds because for  $n/2 \leq p < n$  only  $n-p$  singular values are in the interval  $(0,1)$  and contribute to the product in the left-hand side of Eq. (4.23).  $\square$

As for the projection kernel, a Monte Carlo simulation is performed to verify the consistency of the upper bound presented in this section. In this regard, 3,000 random matrices  $\tilde{\Psi}_j$  are sampled from a Gaussian distribution, as presented in the proof of lemma 4.4, for each value of  $p = 1, \dots, 19$ , with  $n = 20$ . Thus, it is shown in Fig. 3b that the result of lemma 4.7 holds.

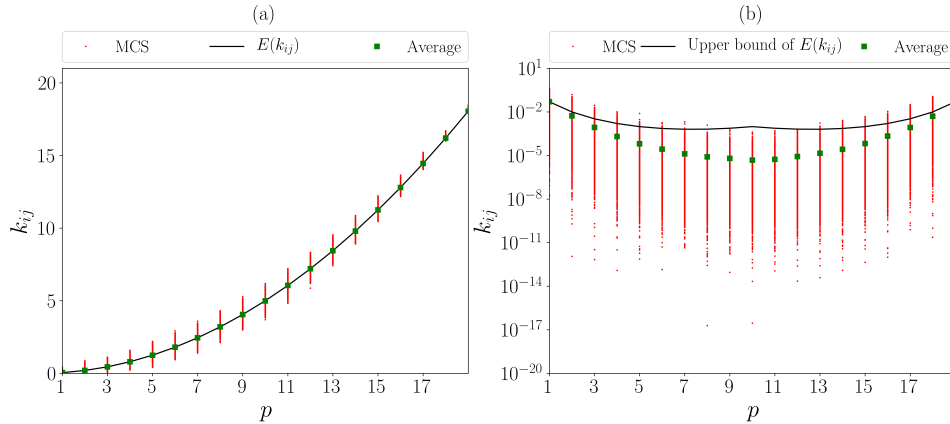


Figure 3: Average from the Monte Carlo simulation and the expected value of the off-diagonal elements of the a) Projection and b) Binet-Cauchy (in log-scale) kernels as functions of  $p$  for  $n = 20$ .

**4.2.3. Kernel dimensionality: comparison.** We see from the previous sections that, the decaying behavior of the off-diagonal terms of the affinity matrix for the Binet-Cauchy kernel causes the kernel matrix to approach an undesirable identity matrix as  $p$  increases up to  $n/2$ . On the contrary, the off-diagonal terms of projection kernel matrix grow with  $p^2$  producing a random walk that mixes well and is suitable for kernel-based dimension reduction, as we will see in the next chapter. Thus, the Binet-Cauchy kernel is generally used when  $p$  is small relative to  $n$  while the projection kernel is used for larger manifold dimensions. In the examples shown later, we are using the projection kernel exclusively for this reason.

**5. Grassmannian diffusion maps.** The conventional diffusion maps [7] defines the similarity in the ambient Euclidean space where only the graphical perception and not the algebraic characteristics of each element in the dataset is taken into consideration. In pattern recognition, for instance, the local geometry of the elements of a

dataset is relevant to characterize the underlying mechanism or features responsible for their shapes in the ambient space. Therefore, the theory of Grassmann manifolds can be used in this context where every element in the dataset can be projected onto a Grassmann manifold where similarity is defined by the affinity between the subspaces and where the redundant features can be discarded. In this regard, a novel nonlinear dimensionality reduction technique, referred to as Grassmannian diffusion maps (GDMs), developed herein merges the diffusion maps framework and the theory of Grassmann manifolds. This technique is composed of both a pointwise and a multi-point dimensionality reduction. The pointwise dimensionality reduction corresponds to the projection of the high-dimensional elements of a dataset onto a Grassmann manifold encoding their local geometric structure. The multipoint dimensionality reduction uses the pairwise affinity of the underlying subspaces of each element of the dataset to reveal an intrinsic structure on the low-dimensional Grassmann manifold. In the following, we elaborate the theoretical underpinnings of the GDMs in a discrete setting. This is followed by a brief algorithmic description of the method.

**5.1. Discrete embedding on Euclidean space.** Considering a set of i.i.d. random samples  $S_N = \{\mathbf{X}_1, \dots, \mathbf{X}_N\}$ , with probability distribution  $f$  and  $\mathbf{X}_i = \mathbb{R}^{n \times m}$  for  $i = 1, \dots, N$ , their projections onto the Grassmann manifold  $\mathcal{G}(p, n)$  are given by  $G_N = \{\mathcal{X}_1, \dots, \mathcal{X}_N\}$ . Next, assuming a positive semi-definite kernel  $k : \mathcal{G}(p, n) \times \mathcal{G}(p, n) \rightarrow \mathbb{R}$  on graph where a random walk  $W_N = (S_N, f, \mathbf{P})$  is performed, one can construct the transition probability matrix  $\mathbf{P}$  resorting to the graph Laplacian normalization. In this regard, the degree matrix is given by the following diagonal matrix  $\mathbf{D} \in \mathbb{R}^{N \times N}$

$$(5.1) \quad D_{ii} = \sum_{j=1}^N k(\mathcal{X}_i, \mathcal{X}_j),$$

where the stationary distribution of the random walk is given by

$$(5.2) \quad \pi_i = \frac{D_{ii}}{\sum_{k=1}^N D_{kk}},$$

Next, the spectral decomposition of the random walk  $W_N$  is presented. First, the kernel matrix  $k_{ij} = k(\mathcal{X}_i, \mathcal{X}_j)$  is normalized as follows

$$(5.3) \quad \kappa_{ij} = \frac{k_{ij}}{\sqrt{D_{ii}D_{jj}}},$$

Therefore, the transition probability  $P_{ij}$  of the random walk  $W_N$  over  $G_N$  is constructed as

$$(5.4) \quad P_{ij}^t = \frac{\kappa_{ij}}{\sum_{k=1}^N \kappa_{ik}}.$$

From the eigendecomposition of  $\mathbf{P}^t$ , one can obtain the first  $q$  eigenvectors  $\{\psi_k\}_{k=0}^q$ , with  $\psi_k \in \mathbb{R}^N$ , and their respective eigenvalues  $\{\lambda_k\}_{k=0}^q$ . In this regard, the diffusion coordinates for the element  $i$  in the dataset are given by

$$(5.5) \quad \Xi_j = (\xi_{j0}, \dots, \xi_{jq}) = (\lambda_0\psi_{j0}, \dots, \lambda_1\psi_{jq}),$$

where  $\psi_{jk}$  corresponds to the position  $j$  of  $\psi_k$ . Next, definition of the diffusion distance for the discrete embedding of the Grassmann manifold in the Euclidean space can be

defined as

$$(5.6) \quad \delta_{ij} = \|p_{ik}^t - p_{jk}^t\|_{L_2(D_{ii}^{-1})} = \left\{ \sum_{k=1}^N [p_{ik}^t - p_{jk}^t]^2 \frac{1}{D_{kk}} \right\}^{\frac{1}{2}},$$

whose spectral representation is given by

$$(5.7) \quad \delta_{ij} = \left\{ \sum_{k=1}^N \lambda_k^{2t} [\psi_{ik} - \psi_{jk}]^2 \right\}^{\frac{1}{2}}.$$

Next, an algorithm summarizing the main steps used in the Grassmannian diffusion maps is presented.

---

**Algorithm 5.1** Grassmannian Diffusion Maps (GDM)

---

**Require:** a set of  $N$  high-dimensional data  $S_N = \{\mathbf{X}_1, \dots, \mathbf{X}_N\}$  with  $\mathbf{X}_i \in \mathbb{R}^{n \times m}$ , and the dimension  $p$  of the Grassmann manifold.

1: **for**  $i \in 1, \dots, N$  **do**

2: Compute the thin Singular Value Decomposition:  $\mathbf{X}_i = \Psi_i \Sigma_i \Phi_i^T$ , where  $\Psi_i \in \mathcal{V}(p, n)$  and  $\Phi_i \in \mathcal{V}(p, m)$ .

3: **end for**

4: For every pair  $[\Psi_i, \Psi_j]$  and  $[\Phi_i, \Phi_j]$  compute the entries of  $k_{ij}$  of the kernel matrices  $k_{ij}(\Psi)$  and  $k_{ij}(\Phi)$ , either using Eq. (4.2) or Eq. (4.4).

5: Compute the composed kernel matrix  $k(\Psi, \Phi)$ . For example:

$$k(\Psi, \Phi) = k_{ij}(\Psi) + k_{ij}(\Phi) \text{ or } k(\Psi, \Phi) = k_{ij}(\Psi) \circ k_{ij}(\Phi), \text{ where } \circ \text{ is the Hadamard product.}$$

6: Compute diagonal matrix  $\mathbf{D} \in \mathbb{R}^{N \times N}$  using  $k(\Psi, \Phi)$  in Eq. (5.1).

7: Compute the normalized kernel matrices using Eq. (5.3) for  $k(\Psi, \Phi)$ .

8: Estimate the transition matrix  $\mathbf{P}^t$  of the Markov chain over the data on the Grassmann manifold.

9: Obtain the eigenvectors and their respective eigenvalues from the eigendecomposition of  $\mathbf{P}^t$  and determine the truncation index  $q$ .

**Ensure:** diffusion coordinates  $\Xi_1, \dots, \Xi_N$ , with  $\Xi_i \in \mathbb{R}^q$ .

---

**6. Grassmannian diffusion maps based data classification.** In this section, a novel data classification technique considering an overcomplete dictionary of the diffusion coordinates is presented. This novel method uses the ability of sparse representation in determining a linear and compact combination of the elements in a dictionary to represent a testing data with the advantage that the data intrinsic geometry is explicitly considered when the Grassmann manifold is mapped into an Euclidean space. Moreover, the amount of stored data is a fraction of the necessary to create a proper dictionary in the conventional approach [42]. To this aim, one can try to find an appropriate sparse representation of a given object by solving a convex optimization problem in the  $l_0$ -norm sense; however, this problem is NP-hard. On the other hand, solving it in the  $l_2$ -norm sense could not yield a sparse solution. To circumvent this limitation, the optimization problem can be relaxed to be solved in the  $l_1$ -norm sense.

In this regard, considering a test sample  $\mathbf{X}_T$  and a training set  $T_N = \{\mathbf{X}_i\}_{i=1}^N$  one can obtain an extended dataset  $T_{N+1} = \{\mathbf{X}_1, \dots, \mathbf{X}_N, \mathbf{X}_T\}$  where the Grassmannian

diffusion maps is applied to obtain the diffusion coordinates  $\Xi_i$  corresponding to  $\mathbf{X}_i$ . Next, the diffusion coordinates of each element in the  $k$ -th class are arranged as the columns of a matrix  $\mathbf{A}_k \doteq [\Xi_{k,1}, \dots, \Xi_{k,N_k}] \in \mathbb{R}^{q \times N_k}$ , where  $N_k$  is the number of elements in class  $k$ , and  $q$  is the truncation index used to define the dimension of the diffusion space. This approach assumes that any test sample given by its diffusion coordinates  $\Xi_T$  will lie in the linear span of the training samples in a given class such that

$$(6.1) \quad \Xi_T = c_{k,1}\Xi_{k,1} + \dots + c_{k,N_k}\Xi_{k,N_k},$$

where  $c_{k,j} \in \mathbb{R}$  with  $j = 1, \dots, N_k$ . Therefore, the dictionary  $\mathbf{A}$  can be constructed concatenating  $k$  matrices  $\mathbf{A}_k$ , such as

$$(6.2) \quad \mathbf{A} \doteq [\mathbf{A}_1, \dots, \mathbf{A}_{N_k}] \in \mathbb{R}^{q \times N}.$$

Therefore, the following underdetermined ( $N > q$ ) linear system is obtained.

$$(6.3) \quad \Xi_T = \mathbf{A}\mathbf{c},$$

where the constant vector  $\mathbf{c} = [0, \dots, 0, c_{k,1}, \dots, c_{k,N_k}, 0, \dots, 0]^T \in \mathbb{R}^N$  has non-zero value in the entries associated to the  $k$ -th class. It is evident that the solution of an underdetermined system is not unique; however, if  $\hat{\mathbf{c}}$  is sufficiently sparse, the exact solution can be recovered with high probability [42]. Moreover, real-life data can be corrupted with noise; thus, an approximation of the solution of the linear system in Eq. (6.3) is sought instead of the exact solution. In this regard, the optimization problem to be solved is given by

$$(6.4) \quad \hat{\mathbf{c}} = \arg \min \|\mathbf{c}\|_1 \quad \text{subject to} \quad \|\mathbf{A}\mathbf{c} - \Xi_T\|_2^2 \leq \epsilon,$$

or by its unconstrained form,

$$(6.5) \quad \hat{\mathbf{c}} = \arg \min \|\mathbf{A}\mathbf{c} - \Xi_T\|_2^2 + \beta \|\mathbf{c}\|_1,$$

where  $\epsilon$  is the error tolerance and  $\beta$  is the regularization constant. As the vector of coefficients  $\hat{\mathbf{c}}$  is determined, one can perform the classification either by assigning the maximum entry of  $\hat{\mathbf{c}}$  to its associated class or by identifying the class yielding the smallest error in the approximation. Clearly, different methods can be employed when performing this task; however, in the last case one can use the information of the subspace structure in the diffusion space. In this regard, a residual can be computed as

$$(6.6) \quad r(k) = \|\mathbf{A}(\mathbf{I}_k^* \circ \hat{\mathbf{c}}_k) - \Xi_T\|_2.$$

Therefore, the classification is performed finding  $k$  minimizing  $r(k)$ , where  $\mathbf{I}_k^* \in \mathbb{R}^q$  is a vector whose elements associated to the  $k$ -th class are equal to one and the rest are zero, and  $\circ$  is the Hadamard product. Next, an algorithm summarizing the steps used in this classification approach is presented.

**Algorithm 6.1** GDM based data classification using sparse representation

**Require:** a set of  $N$  high-dimensional data  $T_N = \{\mathbf{X}_1, \dots, \mathbf{X}_N\}$  with  $\mathbf{X}_i \in \mathbb{R}^{n \times m}$ , the dimension  $p$  of the Grassmann manifold, and a test sample  $\mathbf{X}_T \in \mathbb{R}^{n \times m}$ .

- 1: **for**  $i \in 1, \dots, N$  **do**
- 2:   Compute the thin Singular Value Decomposition:  $\mathbf{X}_i = \Psi_i \Sigma_i \Phi_i^T$ ; where,  $\Psi_i \in \mathcal{V}(p, n)$  and  $\Phi_i \in \mathcal{V}(p, m)$ .
- 3: **end for**
- 4: Compute the thin Singular Value Decomposition:  $\mathbf{X}_T = \Psi_T \Sigma_T \Phi_T^T$ ; where,  $\Psi_T \in \mathcal{V}(p, n)$  and  $\Phi_T \in \mathcal{V}(p, m)$ .
- 5: For the augmented sets  $\Psi = \{\Psi_1, \dots, \Psi_N, \Psi_T\}$  and  $\Phi = \{\Phi_1, \dots, \Phi_N, \Phi_T\}$  compute the entries of  $k_{ij}$  of the kernel matrices  $k_{ij}(\Psi)$  and  $k_{ij}(\Phi)$  using either Eq. (4.2) or Eq. (4.4).
- 6: Compute the composed kernel matrix  $k(\Psi, \Phi)$ . For example:

$$k(\Psi, \Phi) = k_{ij}(\Psi) + k_{ij}(\Phi) \text{ or } k(\Psi, \Phi) = k_{ij}(\Psi) \circ k_{ij}(\Phi), \text{ where } \circ \text{ is the Hadamard product.}$$

- 7: Compute the diffusion coordinates  $\Xi_1, \dots, \Xi_N, \Xi_T$  as in Algorithm 5.1, with  $\Xi_i \in \mathbb{R}^q$ .
- 8: Concatenate the  $\Xi_i$ 's of each class  $k$  as columns of a matrix  $\mathbf{A}_k \in \mathbb{R}^{q \times N_k}$ .
- 9: Create the matrix of training diffusion coordinates  $\mathbf{A} = [\mathbf{A}_1, \dots, \mathbf{A}_{N_k}] \in \mathbb{R}^{q \times N}$ .
- 10: Normalize the columns of  $\mathbf{A}$  and the test sample  $\Xi_T$  to have unit  $l_2$ -norm.
- 11: Solve the convex optimization problem:

$$\hat{\mathbf{c}} = \arg \min \|\mathbf{c}\|_1 \quad \text{subject to} \quad \|\mathbf{A}\mathbf{c} - \Xi_T\|_2^2 \leq \epsilon$$

or alternatively

$$\hat{\mathbf{c}} = \arg \min \|\mathbf{A}\mathbf{c} - \Xi_T\|_2^2 + \beta \|\mathbf{c}\|_1$$

- 12: Compute the residuals for each class  $k$ :  $r(k) = \|\mathbf{A}(\mathbf{I}_k^* \circ \hat{\mathbf{c}}_k) - \Xi_T\|_2$

**Ensure:**  $k(\mathbf{X}_T) = \arg \min_k r(k)$

**7. Examples.** In this section, three problems are considered to assess the performance of the Grassmannian diffusion maps in revealing the intrinsic geometric structure of a dataset for classification purposes. The Grassmannian diffusion maps uses the projection kernel (Eq. (4.4)) because it is not as sensitive as the Binet-Cauchy kernel to the change in the dimensionality of the Grassmann manifold, as demonstrated in section 4.2. In the ensuing analysis, the diffusion coordinates embedding the data into a  $q$ -dimensional Euclidean space are estimated from the eigenvalues  $\{\lambda_k\}_{k=1}^{q+1}$  and eigenvectors  $\{\psi_k\}_{k=1}^{q+1}$  of the transition matrix of the Markov chain defined on the Grassmann manifold. The algorithms of both the conventional and the Grassmannian diffusion maps were implemented in the UQpy software [28] (Uncertainty Quantification with python: <https://uqpyproject.readthedocs.io/en/latest/>), a general purpose Python toolbox for modeling uncertainty in physical and mathematical systems.

**7.1. Structured data on the unit sphere in  $\mathbb{R}^3$ .** Consider a collection  $S_N = \{\mathbf{X}_i\}_{i=1}^N$  of  $N = 10,000$  points defining two cone-like structures in  $\mathbb{R}^3$  as presented in Fig. 4a. In this problem, every point in the set  $S_N$  is composed of three coordinates  $(x_1, x_2, x_3)$  and lie on a surface whose functional form is due to the constraint  $\sin(\phi) = \cos^2(\theta)$ , in spherical coordinates. Therefore, if the radius  $r$  is uniformly dis-

tributed in the interval  $[0, 2]$  a set of random points can be obtained as shown in Fig. 4a, where the color map is determined by the magnitude  $\sqrt{x_1^2 + x_2^2 + x_3^2}$ . This example demonstrates that the Grassmannian diffusion maps can identify a well-defined structure of points on  $\mathcal{G}(1, 3)$  represented by the subspaces spanned by  $\Psi \in \mathcal{V}(1, 3)$  (Fig. 4b). As  $\mathcal{G}(1, 3)$  is represented by an unit sphere in  $\mathbb{R}^3$ , the notion of affinity is given by the angle between pairs of the unit vectors in  $\mathbb{R}^3$ .

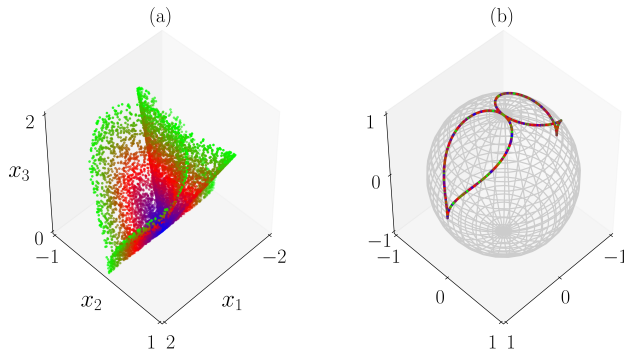


Figure 4: Example 1: (a) Elements of  $S_N$  in  $\mathbb{R}^3$  and colored by their magnitude. (b) Projection onto the Grassmann manifold colored by their magnitude in the ambient space.

Next, Figs. 5a and 5b show the diffusion coordinates for the conventional diffusion maps with a color map defined by the first and the second diffusion coordinates, respectively. On the other hand, Fig. 5c and 5d show the diffusion coordinates for the Grassmannian diffusion maps with a color map defined by the first and the second diffusion coordinates, respectively. One can easily see that the Grassmannian diffusion maps reveals an unidimensional geometric structure connecting the data points, whereas a bidimensional structure is obtained with the conventional diffusion maps. One can observe the influence of the embedded data structure in both the ambient space and the Grassmann manifold using the first two diffusion coordinates to define the color maps. In this regard, for the conventional diffusion maps both the first and the second diffusion coordinates are mapped in the ambient space  $\mathbb{R}^3$  perpendicularly to the canonical directions, as observed in Figs 6a,c. However, when the same diffusion coordinates are mapped on the Grassmann manifold  $\mathcal{G}(1, 3)$  they appear shuffled, and no logical parametrization can be extracted from it, as observed in Figs 6b,d. On the other hand, for the Grassmannian diffusion maps, the first and the second diffusion coordinates in the ambient space  $\mathbb{R}^3$  (Figs. 7a,c) and on the Grassmann manifold  $\mathcal{G}(1, 3)$  (Figs. 7b,d) are clearly structured to align with the intrinsic structure of the data on  $\mathcal{G}(1, 3)$ .

## 7.2. Robust classification of high-dimensional random field data.

In this example, the performance of the GDMs in the classification of high-dimensional random field data is investigated. In this regard, k-means is employed on the obtained diffusion coordinates in order to cluster the most important features influencing the shape of the data in the ambient space. Thus, the elements of a dataset  $S_N = \{\mathbf{X}_1, \dots, \mathbf{X}_N\}$ , with  $N = 3,000$ , are generated with a prescribed rank  $p = 5$ ,

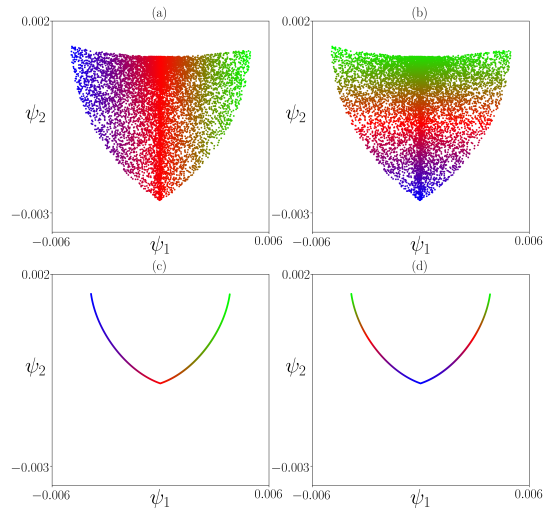


Figure 5: Diffusion coordinates: a) conventional with color map defined by  $\psi_1$  and b)  $\psi_2$ , c) Grassmannian with color map defined by  $\psi_1$  and by d)  $\psi_2$ .

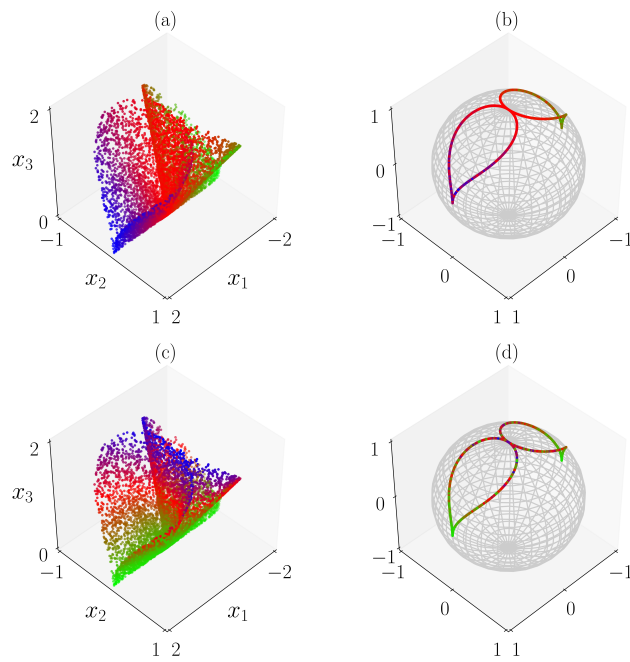


Figure 6: Conventional diffusion maps: color map for  $\psi_1$  in the ambient space a) and on the Grassmann manifold b), and color map for  $\psi_2$  in the ambient space c) and on the Grassmann manifold d).

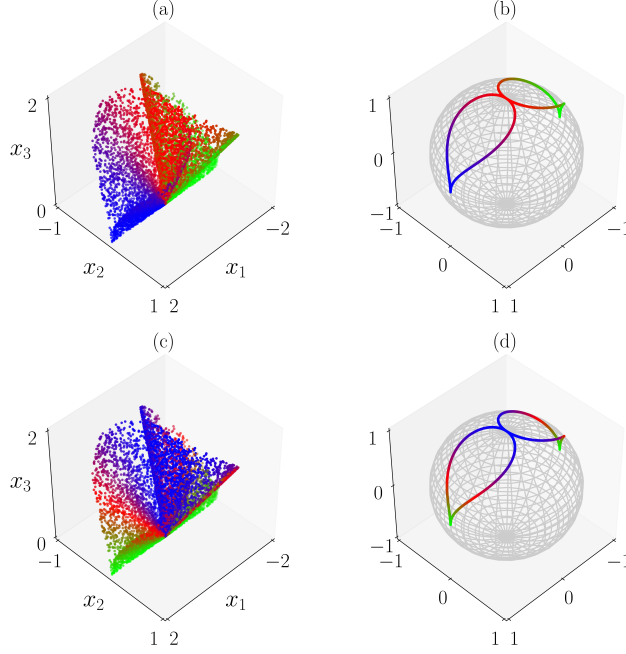


Figure 7: Grassmannian diffusion maps: color map for  $\psi_1$  in the ambient space a) and on the Grassmann manifold b), and color map for  $\psi_2$  in the ambient space c) and on the Grassmann manifold d).

where  $\mathbf{X}_k \in \mathbb{R}^{n \times m}$ , with  $n = m = 40$ , is given by

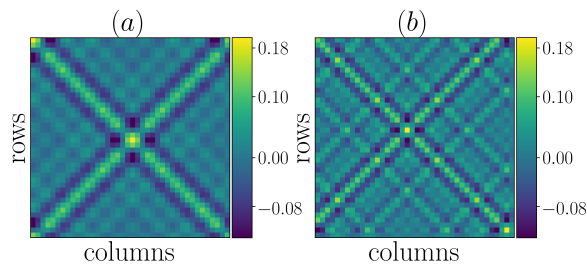
$$(7.1) \quad \mathbf{X}_k = \mathbf{U}_k \mathbf{A}_k \mathbf{U}_k^T,$$

where  $\mathbf{A}_k \in \mathbb{R}^{p \times p}$  is a diagonal matrix whose elements are i.i.d. random numbers with uniform distribution in the interval  $(0, 1]$ , and the entries of  $\mathbf{U}_k \in \mathbb{R}^{n \times p}$  are defined by the following functional form

$$(7.2) \quad u_{ij}^{(k)} = \sqrt{\frac{2}{n}} \cos \left[ \frac{2\pi(j + L_k)}{n} (i - T_k) \right],$$

with  $j = 0, \dots, p$ , and  $i = 0, \dots, n - 1$ . Further,  $T_k$  and  $L_k$  are uniform discrete random variables assuming integer values in the interval  $[0, n - 1]$  and  $[1, \lfloor \frac{n}{2} \rfloor + 1 - p]$ , respectively. It is worth mentioning that the samples  $T_k$  and  $L_k$  are the same for every column of  $\mathbf{U}_k$ , meaning that each element of  $S_N$  is a realization of a two-dimensional random field having a stochastic basis. Fig. 8 shows two realizations of  $\mathbf{X}$  where  $\mathbf{A}_1 = \text{diag}(0.444, 0.828, 0.775, 0.913, 0.981)$ ,  $L_1 = 20$ , and  $T_1 = 3$ ; and  $\mathbf{A}_2 = \text{diag}(0.614, 0.800, 0.184, 0.519, 0.961)$ ,  $L_2 = 38$ , and  $T_2 = 6$ . Moreover,  $p = 5$  is enough to encode information necessary to perform a reliable data classification.

The performance of both techniques are compared by their capacity in revealing the underlying geometry of the random field elements in the set  $S_N$ . In this regard, k-means [22] is utilized to cluster the diffusion coordinates aiming at the classification of random fields by the most relevant features. Based on Eq. (7.2) one expects that

Figure 8: Two realizations of random field elements in  $S_N$ .

$L_k$  will have a strong influence on the shape of the points projected onto  $\mathcal{G}(5, 40)$ . To explore this, the first three diffusion coordinates obtained using the conventional and the Grassmannian diffusion maps are presented in Fig. 9a and in Fig. 9b, respectively; where every point defined by the diffusion coordinates corresponds to an element in  $S_N$ . Moreover, 15 clusters are adopted because 15 values of  $L_k$  are considered. When k-means is applied in the diffusion coordinates obtained by the conventional diffusion maps technique, the dispersion of the diffusion coordinates adversely influences the clustering, as observed in Fig. 9a. This is better observed when the clusters are mapped back to the feature space  $(T_k \times L_k)$  in Fig. 10a, where the shuffled colors are an indication that the classification is only based on the information obtained in the ambient space and no intrinsic characteristics of the elements of the set  $S_N$  are considered. On the other hand, Fig. (9b) shows that the Grassmannian diffusion maps succeed in identifying the intrinsic geometry of the elements in  $S_N$ , where clusters of the Grassmannian diffusion coordinates are clearly delineated. This behavior is evident in Fig. 10b, where the clustering technique is able to identify the elements belonging to the subsets defined by each  $L_k$  with  $k = 1, \dots, 15$ .

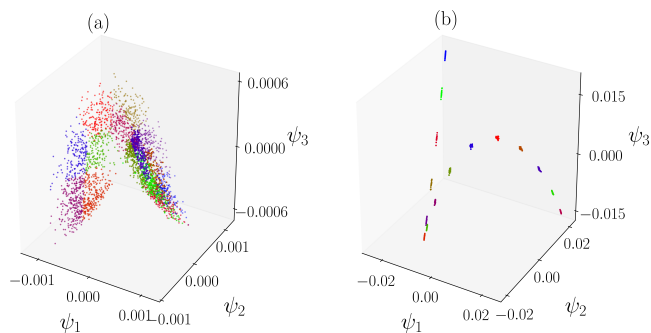


Figure 9: k-means applied on the first three diffusion coordinates (15 clusters): a) Conventional and b) Grassmannian diffusion maps:

**7.3. Sparse representation-based face recognition.** In this example, faces of different subjects are identified using a sparse representation based approach as presented in section 6. The face images used in this experiment were retrieved from the AT&T Database of Faces (AT&T Laboratories Cambridge). This database contains a

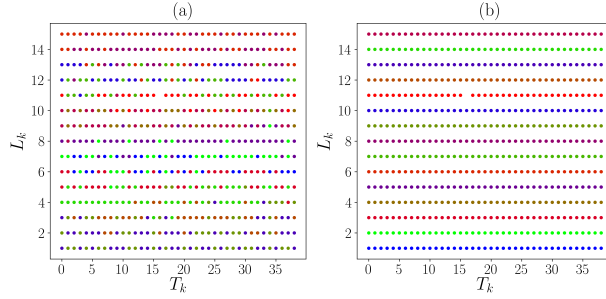


Figure 10: Clusters of the diffusion coordinates mapped in the parameter space  $(T_k \times L_k)$  (a) Conventional diffusion maps (b) Grassmannian diffusion maps.

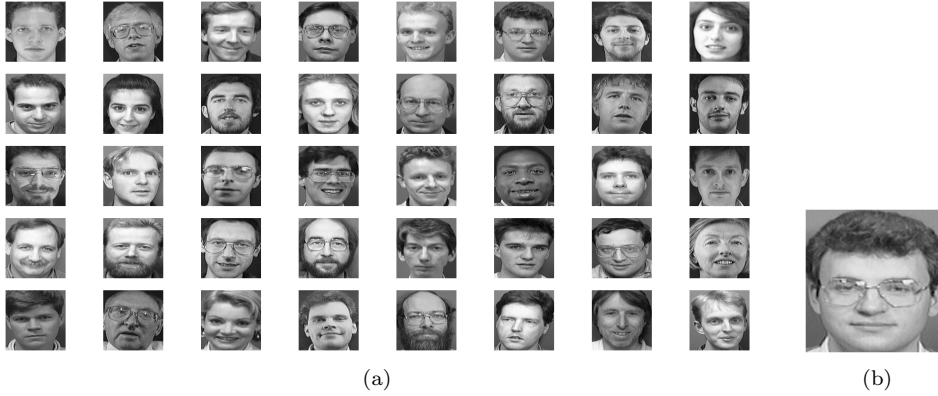


Figure 11: a) One face image of the subject representing each of 40 classes and b) Test face image.

set of 400 face images of 40 subjects, corresponding to 10 face images for each subject taken at different times with variation in the illumination, facial expressions (i.e., open and closed eyes, smiling and not smiling faces), and occlusions (i.e., glasses). Moreover, they were taken against a dark and homogeneous background, the subjects had some limited freedom for some side movement, all images are in grey scale and were resized to the dimension  $200 \times 200$ .

The following experiment consists in using Algorithm 6.1 and its modified version, substituting steps 1-6 by the Gaussian kernel (conventional approach), to recognize the face images in the test sample. In fact, the training set is composed by  $N = 360$  face images (40 classes with 9 face images of the same subject each), and the test set is composed by 40 face images of distinct subjects. First, considering one face image from the test set (Fig. 11b) and assuming that  $p = 4$  can encode the important features of each face image, one can apply both the conventional and the Grassmannian diffusion maps truncating the dimension of the diffusion coordinates in  $q = 20$ .

The facial recognition is performed using either the approximated solution  $\mathbf{c}$  of the underdetermined system or the residuals  $r(k)$ . Moreover, both the constrained and unconstrained convex optimization problems are employed. One can easily notice that the present method informed by the conventional diffusion maps is not able to

recognize the test face image using both  $\mathbf{c}$  (Figs. 12) and  $r(k)$  (Figs. 13) as identification criteria. This observation is also valid for both constrained and unconstrained problems. On the other hand, an exact recognition is obtained for the GDMS-based method using both identification criteria  $\mathbf{c}$  Fig. 14 and  $r(k)$  Fig. 14, and for the constrained and unconstrained optimization problems. It is worth noticing that the solution  $\mathbf{c}$  from the constrained problem for the conventional diffusion maps is not compact. Moreover, the condition number of the transition matrix of the Markov process in the conventional diffusion maps is 849 times larger than the one observed in the Grassmannian diffusion maps, which makes the Grassmannian diffusion maps more stable than its conventional counterpart.

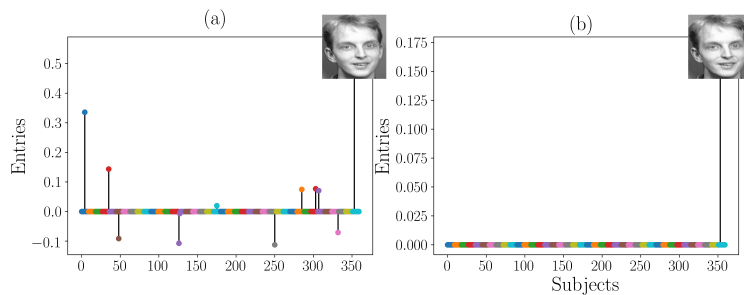


Figure 12: Entries of  $\mathbf{c}$ , with colors defining the 40 classes, for the a) constrained and b) unconstrained minimization problems using the conventional diffusion maps.

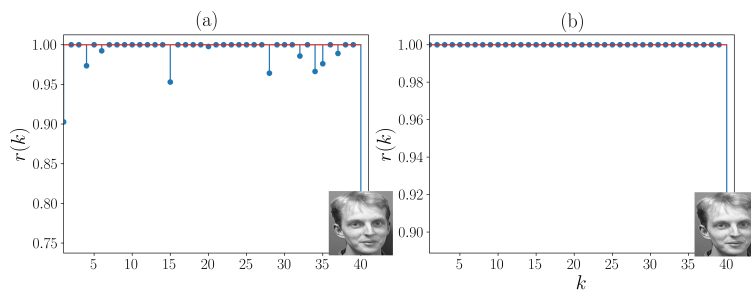


Figure 13: Conventional diffusion maps: residuals  $r(k)$  using the constrained a) and unconstrained b) minimization problems.

Next, the performance of the facial recognition for both the conventional and the Grassmannian diffusion maps is assessed for all 40 subjects in the test set. It is worth mentioning that the conventional diffusion maps only identified 2 subjects when the constrained minimization is employed, and just 1 subject when solving the unconstrained minimization problem. This poor performance can be justified by the low condition number of the transition matrix of the Markov process in the conventional approach. Figure 16 shows how the recognition rate changes for different values of  $p$ . Clearly, one can observe that high recognition rates are obtained even considering  $p = 1$ , however, in the best case scenario a recognition rate of 95% was achieved for

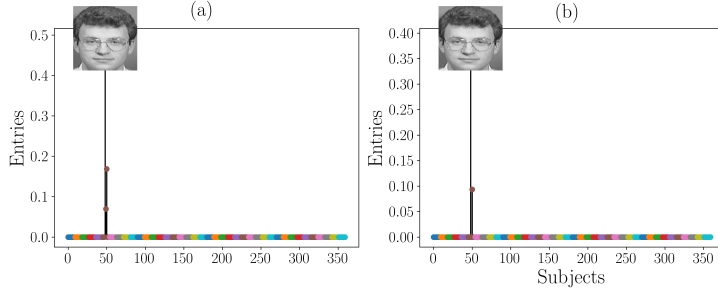


Figure 14: Entries of  $\mathbf{c}$ , with colors defining the 40 classes, for the a) constrained and b) unconstrained minimization problems using the Grassmannian diffusion maps.

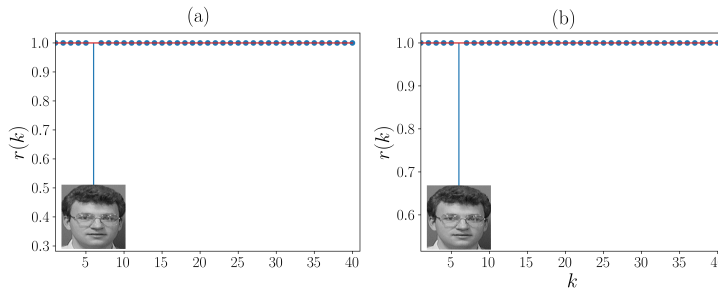


Figure 15: Grassmannian diffusion maps: residuals  $r(k)$  using the constrained a) and unconstrained b) minimization problems.

$p = 12, 13$  and  $14$ . Moreover, it is clear that the recognition rate tends to diminish for very large values of  $p$  (i.e.,  $p > 50$  for instance); however, the use of very larger values of  $p$  is not justified in this kind of application. Moreover, the computational performance of the present technique is comparable with the performance of the sparse representation-based classification method.

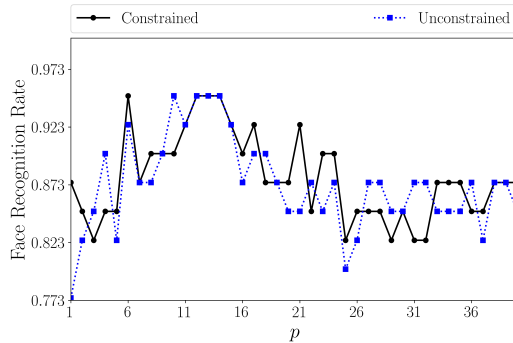


Figure 16: Recognition rate as a function of  $p$  for the recognition approach informed by the GDMs.

**Concluding remarks.** In this paper, a novel dimensionality reduction technique, referred to as Grassmannian diffusion maps, is developed based on the concepts of Grassmann manifold projection and diffusion maps aiming at the characterization and classification of data informed by their intrinsic geometric structure. We demonstrate that an element of a dataset residing in a high-dimensional ambient space can have a representation on a manifold, known as the Grassmann manifold. The proposed method is composed by two main steps, a pointwise dimensionality reduction and a multipoint dimensionality reduction. In the pointwise dimensionality each element of dataset is projected onto a Grassmann manifold where only the most relevant features are kept. On the other hand, the multipoint dimensionality reduction consists in the application of the diffusion maps over the points on the Grassmann manifold to reveal the underlying structure of the dataset. Therefore, instead of using the information in the ambient space, which can be more susceptible to data corruption and external factors (e.g., noise, illumination level in images), the Grassmannian diffusion maps technique uses the information provided by the underlying lower-dimensional subspace of each data point. Furthermore, two lemmas were presented and proved to show the behavior of the first order statistics of the off-diagonal entries of Grassmannian kernels, used in the Grassmannian diffusion maps framework, with changes in its dimensionality. It was demonstrated that the expected value of the off-diagonal entries of the projection kernel grows with order  $\mathcal{O}(p^2)$ , whereas the expected value off-diagonal elements of the Binet-Cauchy kernel decrease drastically with upper bound in the order  $\mathcal{O}(p^p)$ , if  $p < n/2$ ; and grows at a high rate with upper bound in the order  $\mathcal{O}((n-p)^{(n-p)})$ , otherwise.

The performance of the Grassmannian diffusion maps was assessed in three examples where comparison with the conventional diffusion maps were performed to show the potential of this novel approach. The first example contained a theoretical experiment to verify the ability of the present method in finding a structured connection among points projected on the Grassmann manifold represented by the unit sphere in  $\mathbb{R}^3$ . It was shown that the Grassmannian diffusion maps outperforms the conventional method in identifying a well-defined parametric structure of the data when they are projected on the Grassmann manifold  $\mathcal{G}(1, 3)$ . In the second example, a classification experiment with high-dimensional random field data was performed. In particular, the Grassmannian diffusion maps was applied in a dataset of matrices formed by oscillatory functions with random phase and frequency, and k-means was used to cluster the diffusion coordinates corresponding to matrices composed by oscillatory functions with same frequency. The third example presented a practical application of two techniques developed herein, the Grassmannian diffusion maps and the Grassmannian diffusion maps-based data classification using sparse representation. It was demonstrated using the AT&T Database of Faces (AT&T Laboratories Cambridge) that the Grassmannian diffusion maps outperforms the conventional method in identifying 40 face images subject to varying illumination conditions, change in face expressions, and occurrence of occlusions. Moreover, the developed technique presented high recognition rates (95% in the best-case scenario) using a fraction of the information used by conventional face recognition techniques based on sparse representation.

**Acknowledgements.** This work has been supported by the U.S. Department of Energy under grant number DE-SC0020428 and by internal funds provided by Johns Hopkins University.

## REFERENCES

- [1] P.-A. ABSIL, A. EDELMAN, AND P. KOEV, *On the largest principal angle between random subspaces*, Linear Algebra and its Applications, 414 (2006), pp. 288 – 294.
- [2] L. AUSLANDER AND R. MACKENZIE, *Introduction to Differentiable Manifolds*, Dover Books on Mathematics, Dover Publications, 2012.
- [3] M. BALASUBRAMANIAN AND E. L. SCHWARTZ, *The isomap algorithm and topological stability*, Science, 295 (2002), pp. 7–7, <https://doi.org/10.1126/science.295.5552.7a>.
- [4] R. G. BARANIUK, V. CEVHER, AND M. B. WAKIN, *Low-dimensional models for dimensionality reduction and signal recovery: A geometric perspective*, Proceedings of the IEEE, 98 (2010), pp. 959–971.
- [5] E. BEGELFOR AND M. WERMAN, *Affine invariance revisited*, in 2006 IEEE Computer Society Conference on Computer Vision and Pattern Recognition (CVPR'06), vol. 2, 2006, pp. 2087–2094.
- [6] M. BELKIN AND P. NIYOGI, *Laplacian eigenmaps for dimensionality reduction and data representation*, Neural Computation, 15 (2003), pp. 1373–1396.
- [7] R. R. COIFMAN AND S. LAFON, *Diffusion maps*, Applied and Computational Harmonic Analysis, 21 (2006), pp. 5 – 30, <https://doi.org/https://doi.org/10.1016/j.acha.2006.04.006>. Special Issue: Diffusion Maps and Wavelets.
- [8] H. COURANT, R. COURANT, C. COURANT, H. ROBBINS, I. STEWART, AND P. ROBBINS, *What is Mathematics?: An Elementary Approach to Ideas and Methods*, Oxford paperbacks : Mathematics / Oxford paperbacks, Oxford University Press, 1996.
- [9] D. L. DONOHO AND C. GRIMES, *Hessian eigenmaps: Locally linear embedding techniques for high-dimensional data*, Proceedings of the National Academy of Sciences, 100 (2003), pp. 5591–5596, <https://doi.org/10.1073/pnas.1031596100>.
- [10] A. EDELMAN AND N. R. RAO, *Random matrix theory*, Acta Numerica, 14 (2005), p. 233–297.
- [11] C. GAN, J. MAO, Z. ZHANG, AND Q. ZHU, *A tensor compression algorithm using tucker decomposition and dictionary dimensionality reduction*, International Journal of Distributed Sensor Networks, 16 (2020), p. 1550147720916408.
- [12] D. GIOVANIS AND M. SHIELDS, *Uncertainty quantification for complex systems with very high dimensional response using grassmann manifold variations*, Journal of Computational Physics, 364 (2018), pp. 393 – 415, <https://doi.org/https://doi.org/10.1016/j.jcp.2018.03.009>.
- [13] D. G. GIOVANIS AND M. D. SHIELDS, *Data-driven surrogates for high dimensional models using gaussian process regression on the grassmann manifold*, 2020, <https://arxiv.org/abs/2003.11910>.
- [14] P. GRIFFITHS AND J. HARRIS, *Complex Algebraic Varieties*, John Wiley & Sons, 2011, ch. 1, pp. 128–211.
- [15] A. GU, F. SALA, B. GUNEL, AND C. RÉ, *Learning mixed-curvature representations in product spaces*, in International Conference on Learning Representations, 2019.
- [16] J. HAMM AND D. D. LEE, *Grassmann discriminant analysis: A unifying view on subspace-based learning*, in Proceedings of the 25th International Conference on Machine Learning, ICML '08, New York, NY, USA, 2008, Association for Computing Machinery, p. 376–383, <https://doi.org/10.1145/1390156.1390204>.
- [17] J. HAMM AND D. D. LEE, *Extended grassmann kernels for subspace-based learning*, in Advances in Neural Information Processing Systems 21, D. Koller, D. Schuurmans, Y. Bengio, and L. Bottou, eds., Curran Associates, Inc., 2009, pp. 601–608.
- [18] M. HARANDI, R. HARTLEY, C. SHEN, B. LOVELL, AND C. SANDERSON, *Extrinsic methods for coding and dictionary learning on grassmann manifolds*, International Journal of Computing Vision, 114 (2015), p. 113–136, <https://doi.org/https://doi.org/10.1007/s11263-015-0833-x>.
- [19] M. T. HARANDI, M. SALZMANN, S. JAYASUMANA, R. HARTLEY, AND H. LI, *Expanding the family of grassmannian kernels: An embedding perspective*, 2014, <https://arxiv.org/abs/1407.1123>.
- [20] P. HARTMAN, *On the local uniqueness of geodesics*, American Journal of Mathematics, 72 (1950), pp. 723–730.
- [21] I. JOLLIFFE, *Principal Component Analysis*, Springer Berlin Heidelberg, 2011, pp. 1094–1096, [https://doi.org/10.1007/978-3-642-04898-2\\_455](https://doi.org/10.1007/978-3-642-04898-2_455).
- [22] S. P. LLOYD, *Least squares quantization in pcm*, IEEE Transactions on Information Theory, 28 (1982), pp. 129–137.
- [23] J. MARUSKIN, *Introduction to Dynamical Systems and Geometric Mechanics*, Solar Crest Publishing, LLC, 2012.

- [24] J. MIAO AND A. BEN-ISRAEL, *On principal angles between subspaces in  $m$* , Linear Algebra and its Applications, 171 (1992), pp. 81 – 98.
- [25] K. R. MOON, J. S. STANLEY, D. BURKHARDT, D. VAN DIJK, G. WOLF, AND S. KRISHNASWAMY, *Manifold learning-based methods for analyzing single-cell rna-sequencing data*, Current Opinion in Systems Biology, 7 (2018), pp. 36 – 46.
- [26] K. R. MOON, D. VAN DIJK, Z. WANG, W. CHEN, M. J. HIRN, R. R. COIFMAN, N. B. IVANOVA, G. WOLF, AND S. KRISHNASWAMY, *Phate: A dimensionality reduction method for visualizing trajectory structures in high-dimensional biological data*, bioRxiv, (2017), <https://doi.org/10.1101/120378>, <https://arxiv.org/abs/https://www.biorxiv.org/content/early/2017/03/24/120378.full.pdf>.
- [27] R. J. MUIRHEAD, *Aspects of multivariate statistical theory*, John Wiley & Sons, 1982.
- [28] A. OLIVIER, D. GIOVANIS, B. AAKASH, M. CHAUHAN, L. VANDANAPU, AND M. SHIELDS, *Uppy: A general purpose python package and development environment for uncertainty quantification*, Journal of Computational Science, (2020), p. 101204.
- [29] J. OPREA, *Differential Geometry and Its Applications*, Classroom resource materials, Mathematical Association of America, 2007.
- [30] S. T. ROWEIS AND L. K. SAUL, *Nonlinear dimensionality reduction by locally linear embedding*, Science, 290 (2000), pp. 2323–2326, <https://doi.org/10.1126/science.290.5500.2323>.
- [31] B. SCHÖLKOPF, A. SMOLA, AND K. MÜLLER, *Nonlinear component analysis as a kernel eigenvalue problem*, Neural Computation, 10 (1998), pp. 1299–1319.
- [32] C. SOIZE AND R. GHANEM, *Probabilistic learning on manifolds*, 2020, <https://arxiv.org/abs/2002.12653>.
- [33] S. SOMMER, T. FLETCHER, AND X. PENNEC, *1 - introduction to differential and riemannian geometry*, in Riemannian Geometric Statistics in Medical Image Analysis, X. Pennec, S. Sommer, and T. Fletcher, eds., Academic Press, 2020, pp. 3 – 37.
- [34] J. B. TENENBAUM, V. D. SILVA, AND J. C. LANGFORD, *A global geometric framework for nonlinear dimensionality reduction*, Science, 290 (2000), pp. 2319–2323, <https://doi.org/10.1126/science.290.5500.2319>.
- [35] P. TURAGA, A. VEERARAGHAVAN, AND R. CHELLAPPA, *Statistical analysis on stiefel and grassmann manifolds with applications in computer vision*, in 2008 IEEE Conference on Computer Vision and Pattern Recognition, 2008, pp. 1–8.
- [36] J. UH, M. A. KHAN, AND C. HUA, *Four-dimensional MRI using an internal respiratory surrogate derived by dimensionality reduction*, Physics in Medicine and Biology, 61 (2016), pp. 7812–7832.
- [37] L. J. P. VAN DER MAATEN AND G. E. HINTON, *Visualizing data using t-sne*, Journal of Machine Learning Research, 9 (2008), p. 2579–2605.
- [38] S. VISHWANATHAN AND A. SMOLA, *Binet-cauchy kernels. advances in neural information processing systems*, in Advances in Neural Information Processing Systems, no. 17 in NIPS '04, 2004.
- [39] B. WANG, Y. HU, J. GAO, Y. SUN, AND B. YIN, *Low rank representation on grassmann manifolds: An extrinsic perspective*, 2015, <https://arxiv.org/abs/1504.01807>.
- [40] R. WANG, X. WU, AND J. KITTLER, *Graph embedding multi-kernel metric learning for image set classification with grassmann manifold-valued features*, IEEE Transactions on Multimedia, (2020), pp. 1–1.
- [41] Y.-C. WONG, *Differential geometry of grassmann manifolds*, in Proceedings of the National Academy of Sciences of the United States of America, 1967, p. 589–594.
- [42] J. WRIGHT, A. Y. YANG, A. GANESH, S. S. SASTRY, AND Y. MA, *Robust face recognition via sparse representation*, IEEE Transactions on Pattern Analysis and Machine Intelligence, 31 (2009), pp. 210–227.
- [43] J. WU, L. HUANG, W. LI, H. CHAN, C. LIU, AND R. GAU, *Sparse subspace clustering with linear subspace-neighborhood-preserving data embedding*, in 2020 IEEE 11th Sensor Array and Multichannel Signal Processing Workshop (SAM), 2020, pp. 1–5.
- [44] W. YAN, Q. SUN, H. SUN, AND Y. LI, *Joint dimensionality reduction and metric learning for image set classification*, Information Sciences, 516 (2020), pp. 109 – 124.
- [45] K. YE AND L.-H. LIM, *Schubert varieties and distances between subspaces of different dimensions*, 2014, <https://arxiv.org/abs/1407.0900>.
- [46] K. YE, K. S.-W. WONG, AND L.-H. LIM, *Optimization on flag manifolds*, 2019, <https://arxiv.org/abs/1907.00949>.
- [47] R. ZIMMERMANN, *Manifold interpolation and model reduction*, 2019, <https://arxiv.org/abs/1902.06502>.